



Cite this: *CrystEngComm*, 2020, 22, 2483

Synthesis of Na₂Ti₃O₇ nanorods by a V-assisted route and investigation of their battery performance

S. Altin,^{*a} S. Demirel,^b E. Oz,^a E. Altin,^c C. Hetherington,^d A. Bayri^a and S. Avci ^{*e}

We report the V-assisted synthesis of Na₂Ti₃O₇ nanorods *via* a conventional solid state reaction technique. Energy dispersive X-ray spectroscopy (EDS) mapping showed that V-ions are not incorporated into the main structure of the nanorods but rather V behaves as a flux agent during the growth of the nanorods. The cyclic voltammetry (CV) analysis of the samples shows changes in the redox peaks as a function of V content. Our detailed *ex situ* X-ray diffraction (XRD), Raman spectroscopy, scanning electron microscopy (SEM), transmission electron microscopy (TEM) and X-ray absorption spectroscopy (XAS) analyses after 1000 cycles show that the degradation mechanism is the formation of various titanium oxide impurity phases which inhibits the Na-ion diffusion.

Received 11th December 2019,
Accepted 23rd February 2020

DOI: 10.1039/c9ce01955c

rsc.li/crystengcomm

1. Introduction

Although Li-ion batteries have conquered the portable electronics market, their limitations due to the high cost and availability of Li have prevented them to be used in large scale applications. Na is a promising alternative due to its natural abundance and similar intercalation properties to Li. Despite their rich redox chemistry, Na-ion batteries have lower energy density and voltage than Li-ion batteries. More studies have to be performed to optimize the electrode materials in the Na-ion battery field in order to catch up with the Li-ion battery technology. Most studies have been related to positive electrodes; however, less attention has been paid to the negative electrodes for Na-ion batteries.^{1,2}

The performance of a battery depends on the working potential which is the difference between the potentials of the positive and negative electrodes. Therefore, a low ionization voltage, *i.e.* between 0 and 2 V, is a good criterion for anode materials. Among the various types of anode materials for Na-ion batteries such as carbonaceous materials, Na alloys and compounds and Ti-based compounds,³ Na₂Ti₃O₇ is promising due to its very low potential (0.3 V).⁴ Na₂Ti₃O₇ consists of zigzag layers of TiO₆ octahedra with a monoclinic crystal structure (*P*2₁/*m* space group). Up to 3.5 Na ions per formula unit can be intercalated into the interlayer space, leading to a

theoretical capacity of 311 mA h g⁻¹.⁵ Experimental capacity values are far from the theoretical value for now, therefore extensive research efforts are required to improve the capacity of Na₂Ti₃O₇. Na₂Ti₃O₇ can be synthesized *via* various techniques in several forms: nanosheet⁶ and nanorod⁷ forms *via* hydrothermal synthesis, bulk form from solid state reactions⁴ and microsphere form with a spray drying method.⁸ The capacity value of Na₂Ti₃O₇ is very sensitive to its synthesis technique and its morphology. For instance, a capacity value of 188 mA h g⁻¹ at a current rate of 0.1 C was reached by solid state synthesis.⁹ However, the capacity decreases to 60 mA h g⁻¹ for the 60th cycle. Man *et al.* have synthesized sheet-like Na₂Ti₃O₇ materials by solid state synthesis with hollow sphere TiO₂ as the Ti source. Electrochemical measurements show that an initial charge capacity of 191 mA h g⁻¹ at a 0.1 C rate decreases to 101 mA h g⁻¹ after 50 cycles.¹⁰ Ding *et al.* synthesized carbon-coated Na₂Ti₃O₇ *via* the solid state reaction method. They report an initial discharge capacity of 215 mA h g⁻¹ at a 20 mA current rate which shows a sharp decrease for the 25th cycle down to ~60 mA h g⁻¹.¹¹ All these solid-state synthesis reports yield Na₂Ti₃O₇ in bulk form. However, the effects of nanosized electrode materials on battery performance have been reported repeatedly^{12–14} and conventional solid-state synthesis is useful for large scale production due to its simplicity. Therefore, it is important to synthesize Na₂Ti₃O₇ in nanosize *via* solid state synthesis. There has been one recent study reporting synthesis of a mixture of Na₂Ti₃O₇/Na₂Ti₆O₁₃ nanorods *via* the solid state reaction by adding carbon during synthesis.¹⁵ These nanorods showed promising electrochemical performance especially at high rates (95Na₂Ti₃O₇/5Na₂Ti₆O₁₃ with an initial specific discharge

^a Department of Physics, Inonu University, Malatya, 44280, Turkey.

E-mail: serdar.altin@inonu.edu.tr

^b Department of Electricity and Energy, Igdir University, Igdir, 76000, Turkey

^c IBTAM, Inonu University, Malatya, 44280, Turkey

^d Department of Chemistry, Lund University, Lund, 22100, Sweden

^e Department of Engineering Physics, Istanbul Medeniyet University, Istanbul, 34700, Turkey. E-mail: sevda.avci@medeniyet.edu.tr



capacity of 92 mA h g⁻¹ at a 5 C rate). In this work we report a new route for solid state synthesis of Na₂Ti₃O₇ nanorods by adding vanadium. Our results confirm that the V ions do not diffuse into the lattice of Na₂Ti₃O₇ nanorods, instead they behave as a flux agent in the main matrix that assists the formation of the nanorods. We have tested the electrochemical properties of Na₂Ti₃O₇ nanorods in Na-ion batteries and used *ex situ* characterization techniques to study their capacity fade mechanism.

2. Experimental section

Nominal Na₂Ti_{3-x}V_xO₇ compounds, where $x = 0.0, 0.025, 0.05, 0.1,$ and $0.15,$ were synthesized *via* the solid state reaction method. Powders of 99% purity Na₂CO₃, TiO₂, and V₂O₅ were used as starting materials. The mixed powder was heated at 800 °C in air for 16 hours to remove the carbonates. After furnace cooling, the powder was mixed with an agate mortar and kept at 800 °C for 12 hours to obtain the final compositions.

X-ray diffraction (XRD) measurements were performed using CuK α ($\lambda = 1.5405$ Å) radiation with a Siemens Bruker D5000 computer-controlled X-ray diffractometer at the University of Illinois at the Urbana-Champaign Materials Research Laboratory. The data were collected at a constant scanning rate of 2° min⁻¹ at $2\theta = 2$ –80°. Unit cell parameters were determined by the Rietveld refinement technique using the comprehensive General Structure Analysis System II (GSAS II) software.¹⁶

For the surface morphology analysis, a JEOL 6060LV general purpose scanning electron microscope (SEM) was used at the University of Illinois at the Urbana-Champaign Materials Research Laboratory. For the transmission electron microscopy (TEM) analysis, a JEOL 3000F with an energy dispersive X-ray spectroscopy (EDS) attachment was used at 300 kV at Lund University, Sweden. X-ray absorption fine structure (XAFS) analysis of the samples was performed at beamline 64 at DESY synchrotron in Germany.

Pure Na metal was used as a counter electrode for electrochemical characterization. The nominal Na₂Ti_{3-x}V_xO₇ compositions where $x = 0, 0.025, 0.05, 0.1,$ and 0.15 were mixed with polyvinylidene fluoride (PVDF) and carbon black (CB) with a ratio of 70 : 15 : 15 for CR2032 coin cells. The coin cells were pressed in an Ar gas filled glove box. Charge-discharge and cyclic voltammetry measurements were performed using a Bio-logic VPM3. Charge-discharge measurements were conducted at 0.2, 0.5, 1 and 2 C rates in the 0.5–2 V range. CV measurements were taken at 0.1 mV s⁻¹ in the 0.1–2 V range.

3. Results and discussion

3.1. Growth of the nanorods

The growth of nano-size rod-like crystals is important in electrochemical processes due to their high surface area and short diffusion distances.^{17,18} Also, a crystalline structure is

essential since ion diffusion occurs through certain crystallographic directions and planes.¹⁹ Although Na₂Ti₃O₇ has been synthesized in nanorod form *via* various chemical techniques, solid state synthesis yields bulk materials for this compound.^{20,21} Sauvet *et al.* have reported the single phase formation temperature of Na₂Ti₃O₇ to be 800 °C based on thermogravimetric and thermal differential analysis data.²² Fig. 1(a) shows the XRD data of nominal Na₂Ti_{3-x}V_xO₇ compositions annealed at 850 °C. All the samples have the Na₂Ti₃O₇ phase as the main phase. Fig. 1(b) shows the Rietveld refinement of the Na₂Ti₃O₇ structure for the $x = 0.1$ sample.

We have used the XRD data to calculate the lattice parameters and unit cell volume of the samples and observed that addition of V does not cause a significant change in the cell parameters, as listed in Table 1. This can also be confirmed by the XRD data shown in Fig. 1(a) where the peaks do not shift noticeably upon V addition. One possible explanation is the very small difference between the ionic

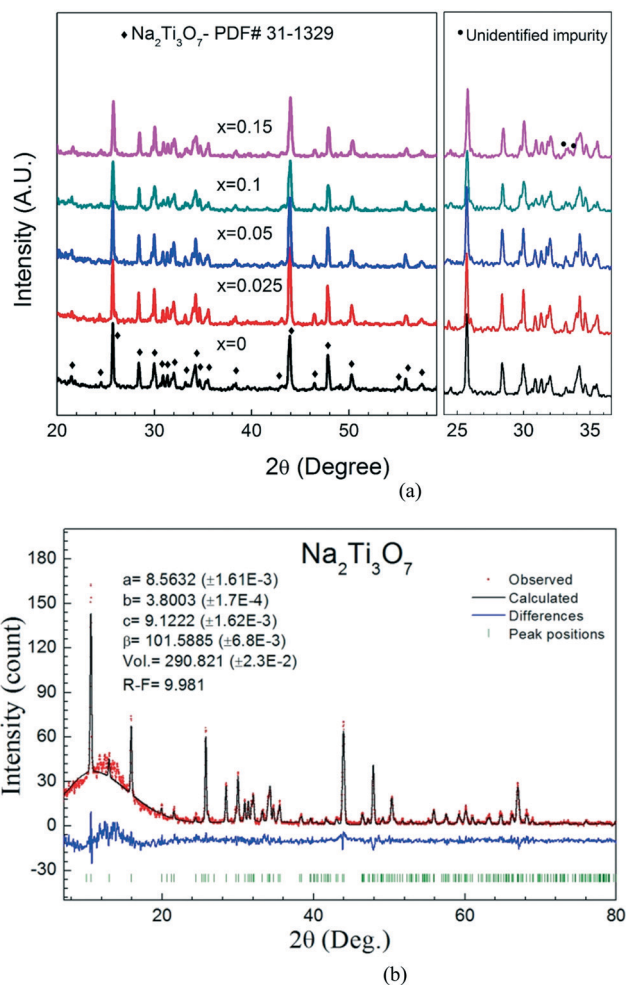


Fig. 1 (a) XRD data of Na₂Ti_{3-x}V_xO₇ samples with nominal compositions where $x = 0.00, 0.025, 0.05, 0.10$ and $0.15.$ (b) Rietveld refinement of the Na₂Ti₃O₇ structure for the nanorods scraped from the surface of the main matrix of the $x = 0.1$ sample.

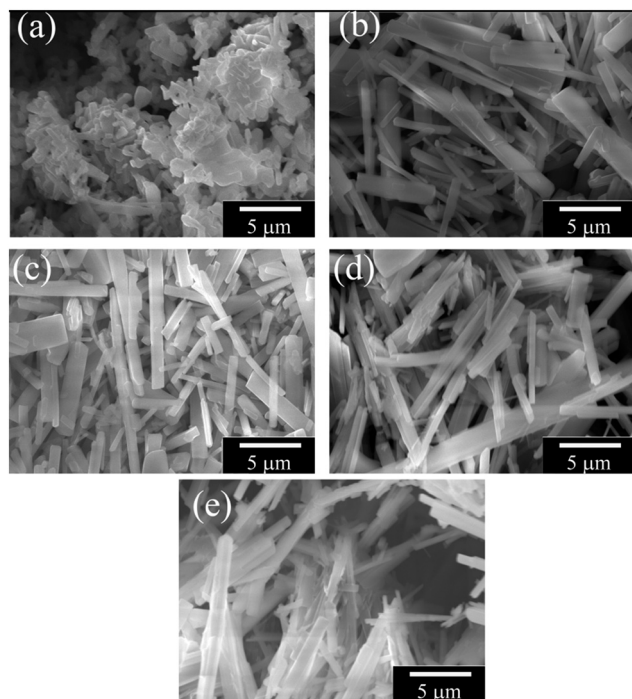


Table 1 Cell parameters of nominal $\text{Na}_2\text{Ti}_{3-x}\text{V}_x\text{O}_7$ compositions determined via Rietveld refinement

Sample	a (Å)	b (Å)	c (Å)	Volume (Å ³)
0.00	8.5685(14)	3.80054(22)	9.1252(15)	291.125(41)
0.025	8.5613(11)	3.80255(15)	9.1274(16)	291.066(26)
0.05	8.5619(11)	3.80204(12)	9.1264(11)	291.026(15)
0.10	8.5652(16)	3.80156(17)	9.1208(16)	290.945(22)
0.15	8.5644(13)	3.80129(15)	9.1252(14)	291.017(19)

radii of Ti^{4+} and V^{4+} ions (for 6-coordinations, the ionic radii are 74.5 pm and 72 pm, respectively). Another possible explanation is that the V ions do not incorporate with the lattice of $\text{Na}_2\text{Ti}_3\text{O}_7$, instead they form a vanadium-containing impurity phase. We have detected impurity peaks in our XRD data; however, we could not identify these peaks due to their low intensity. These impurity peaks are not present in the samples with low V content ($x = 0.025$) and start appearing at the $x = 0.05$ sample. We have performed EDS analysis to observe if V is present in the nanorods as discussed later in this section.

Growth of crystals is usually initiated by a nucleus which is formed on the bulk part of the sample. Grain shapes of materials are directly related to the thermodynamic conditions of the environment such as temperature, pressure, internal energy, *etc.* A triggering mechanism is needed for the formation of rod-like grains since the rod-like grain formation requires more energy than that of the flake-like grains due to their high surface area.²³ In our case, addition of V triggers the formation of $\text{Na}_2\text{Ti}_3\text{O}_7$ nanorods. Fig. 2

**Fig. 2** SEM images of $\text{Na}_2\text{Ti}_{3-x}\text{V}_x\text{O}_7$ samples where (a) $x = 0$, (b) $x = 0.025$, (c) $x = 0.05$, (d) $x = 0.1$ and (e) $x = 0.15$.

shows the SEM images of nominal $\text{Na}_2\text{Ti}_{3-x}\text{V}_x\text{O}_7$ compounds. While the V-free sample ($x = 0.0$) does not contain any nanorods, even addition of a tiny amount of V ($x = 0.025$) activates the formation of nanorods.

Fig. 3 shows the TEM images of a nanorod and its diffraction pattern. The nanorod shows the single crystalline structure with growth along the b -axis. Values of the interplanar spacings were measured from the high resolution image and the obtained values (0.83 nm and 0.39 nm) correspond within error to the values calculated from the XRD data (Table 1).

The growth of one-dimensional crystals in the form of nanorods is a curious subject in materials science. There are several suggested models for the growth of these nanorods such as vapor–solid–liquid mechanisms, defect-assisted growth, *etc.*^{24–26} Based on our results, the most appropriate mechanism to explain the growth of $\text{Na}_2\text{Ti}_3\text{O}_7$ nanorods is the defect-assisted growth. According to this model, incorporation of V in the lattice forms a defect and such defects on the surface of the main matrix causes formation of nuclei for the grains. The grains start to grow on the nuclei and the V defect does not diffuse into the structure of the nanorods; rather it behaves as a catalytic role in the growth process.²⁷ To test this hypothesis we have performed EDS analysis to observe if the V-ions are present in the nanorods. We examined several nanorods and found that V-ions do not incorporate the structure of the nanorods. Fig. 4 shows investigations into one nanorod as an example. The STEM image was used to define a region for recording EDS spectra and mapping the main elements Na, Ti and O. The sum spectra were obtained from the mapping data and used to calculate atomic percentages. These were Na 16%, Ti 16%, O 68% and V 0.1%. The discrepancy between these numbers and the formula $\text{Na}_2\text{Ti}_3\text{O}_7$ probably has two causes. One is that the calculated percentages depend on the value of thickness incorporated into the calculation; we estimated 200 nm but over the area of the map there is a large variation and hence uncertainty. The second is that on other occasions where spot analyses were attempted, we observed material loss at the site of the electron probe. The percentage for V was given at 0.1%. Values below around 1% mean that one normally concludes that an element is below the detection limit. The analysis of this EDS spectrum is complicated by an overlap of the V K_{α} peak at 4.95 keV and the Ti K_{β} peak at 4.93 keV. The strong Ti K_{α} signal at 4.51 keV and the weaker Ti K_{β} peak are clearly visible. The locations of V K peaks, where they should be present, are marked in red in Fig. 4. The, V K_{β} peak location at 5.43 keV must be examined instead of the main V K_{α} peak. At 5.43 keV, there was no sign of a peak which allows us to say that V is not detected. We conclude that V-ions are not incorporated but instead play a catalytic role in the nanorod growth similar to the growth of $\text{Na}_{0.44}\text{MnO}_2$ nanorods as discussed in detail in our previous report.²⁸

Fig. 5(a) shows the Ti–K edge XANES spectra of the samples of the nominal $\text{NaV}_x\text{Ti}_{3-x}\text{O}_2$ compounds where $x = 0.00–0.25$. The XANES data show seven different featured peaks or kinks



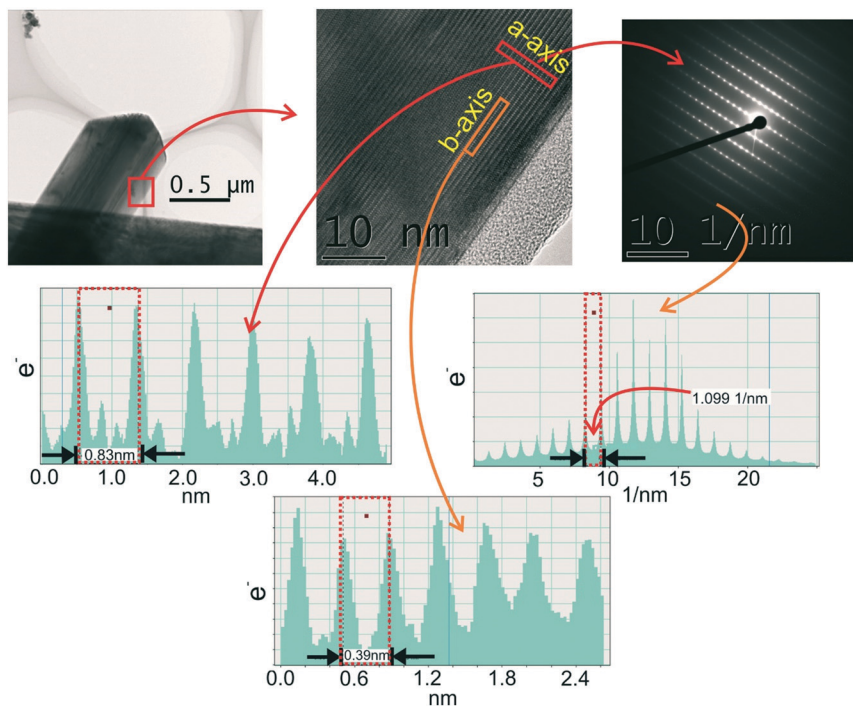


Fig. 3 TEM images of a nanorod synthesized by V-substitution at the $x = 0.05$ level and before cycling. Analysis of the high resolution image and diffraction patterns taken from the same area give spacings along the b -direction as 0.39 nm and along the a -direction as 0.83 nm.

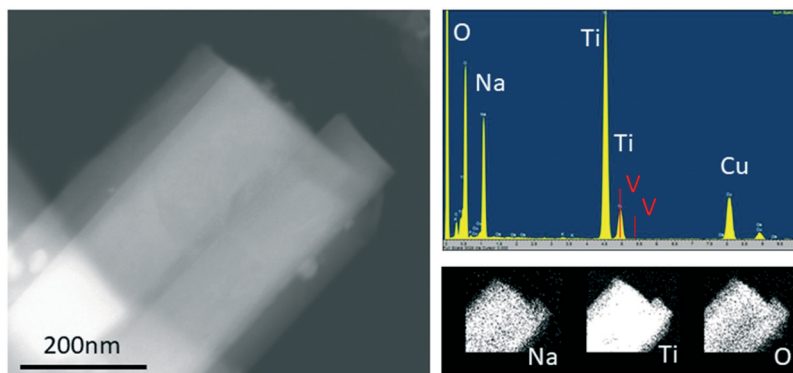


Fig. 4 TEM-EDS image of a nanorod of the nominal $\text{Na}_2\text{Ti}_{3-x}\text{V}_x\text{O}_7$ composition where $x = 0.05$. On the left is a STEM dark field image. Upper right: The sum spectra recorded during mapping; peaks for O K_{α} , Na K_{α} , and Ti K_{α} are visible (Cu comes from the copper grid used as a sample holder). Lower right: The elemental maps indicate a uniform composition across the nanorod.

as labelled in Fig. 5(a). A. Niltharach *et al.* stated that A_1 is related to the quadrupole transition from $1s$ to the t_{2g} level of the TiO_6 octahedron, A_2 and A_3 can be explained by the transition from $1s$ to $3d$ orbitals and B is attributed to the transition from $1s$ to $4p$ orbitals (detailed information can be found in ref. 29 and 30).

The crystal structure of $\text{Na}_2\text{Ti}_3\text{O}_7$, obtained from Rietveld refinement, shown in Fig. 5(b), consists of three Ti sites, seven oxygen sites and two Na sites. Hennig *et al.* have reported that bond lengths obtained from the XRD data can be less reliable than the values obtained from the EXAFS data.³¹ We have used the Fourier transform (FT) EXAFS data to confirm the interatomic parameters (bond lengths)

obtained from the XRD data. In the FT EXAFS data (Fig. 5(c)), the peaks are labelled P_1 , P_2 , P_3 , P_4 and P_5 (Fig. 5(d)) and corresponding bond types (listed in Table 2) are gathered from the XRD data. Each peak of the FT data consists of several bonds in the structure. Although the peak values of the FT EXAFS data provide the bond lengths of ions, the peak widths explain the statistical distribution of the bond lengths.

3.2. Battery performance

Fig. 6a–e show the plot of the galvanostatic test profiles of nominal $\text{Na}_2\text{Ti}_{3-x}\text{V}_x\text{O}_7$ compounds up to 1000 cycles at a 0.5



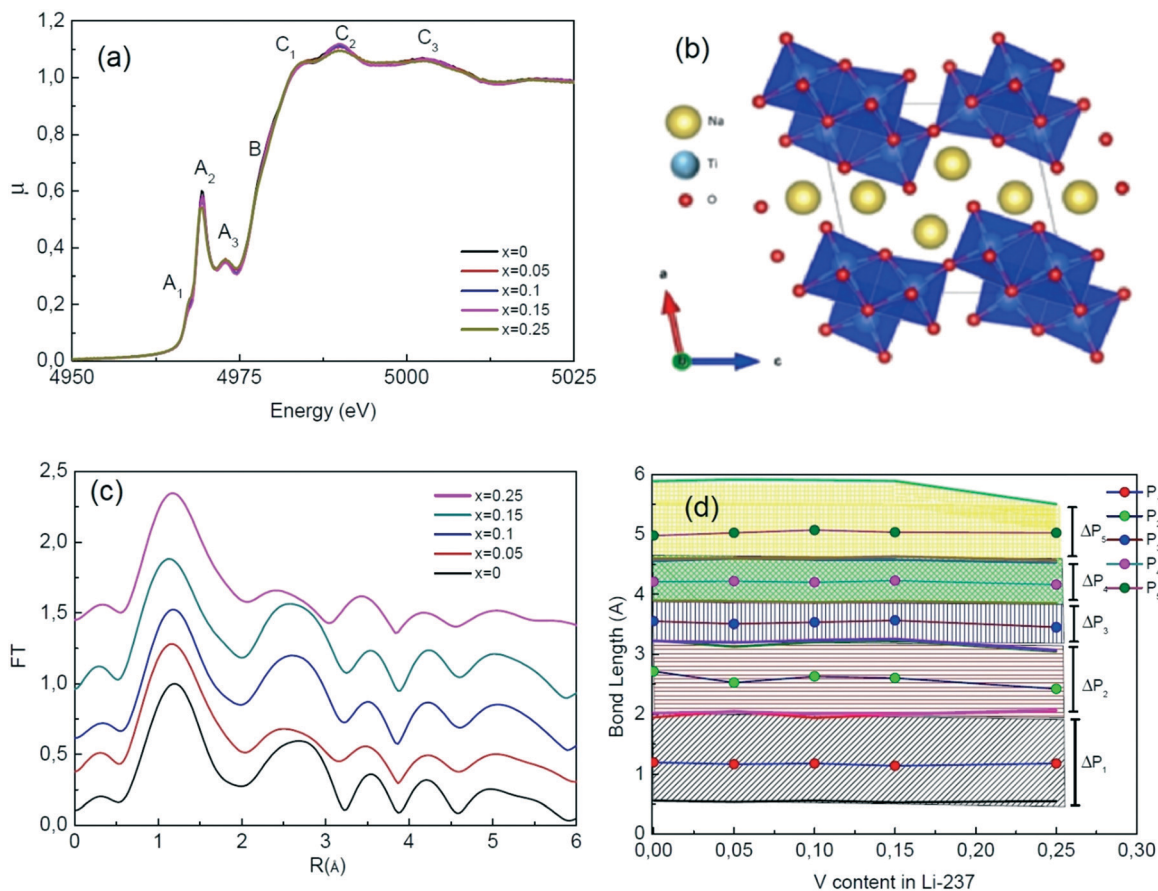


Fig. 5 (a) XANES data of nominal $\text{Na}_2\text{Ti}_{3-x}\text{V}_x\text{O}_7$ samples where $x = 0.0, 0.025, 0.05, 0.1$ and 0.15 , (b) crystal structure of $\text{Na}_2\text{Ti}_3\text{O}_7$, (c) FT XANES data of $\text{Na}_2\text{Ti}_{3-x}\text{V}_x\text{O}_7$ and (d) peak positions and sizes ($\Delta P = P_{\text{end}} - P_{\text{start}}$) obtained from the FT data depending on the V content.

Table 2 The relationship between the FT peak positions and bond types

Label in the FT data	Peak start (Å)	Peak end (Å)	Peak value (Å)	Bond types
P ₁	0.54	1.98	1.15	Ti ₁ -O ₁ , Ti ₁ -O ₂ , Ti ₂ -O ₂ , Ti ₂ -O ₃ , Ti ₃ -O ₄ , Ti ₁ -O ₅ , Ti ₂ -O ₆ , Ti ₃ -O ₁
P ₂	2.02	3.21	2.6	Ti ₂ -Ti ₃ , Ti ₂ -O ₄ , Ti ₃ -O ₇ , Ti ₂ -O ₅ , Ti ₁ -O ₆ , Ti ₁ -O ₇
P ₃	3.25	3.87	3.45	Ti ₃ -O ₆ , Ti ₂ -O ₇ , Ti ₁ -Ti ₂ , Ti ₁ -Na ₁ , Ti ₂ -Na ₁
P ₄	3.90	4.56	4.2	Ti ₂ -O ₁ , Ti ₃ -O ₃ , Ti ₁ -Na ₂ , Ti ₁ -Na ₂ , Ti ₃ -Na ₂ , Ti ₃ -O ₂ , Ti ₁ -O ₃
P ₅	4.63	5.93	5.05	Ti ₁ -O ₄ , Ti ₃ -Na ₁ , Ti ₁ -Ti ₃

C rate. The pristine compound, $\text{Na}_2\text{Ti}_3\text{O}_7$, shows similar battery performance to that reported in the literature.³² A significant decrease in the capacity values upon increasing the cycle number is observed for most of the samples including the pristine compound. The lowest capacity fade after 1000 cycles is obtained for the $x = 0.1$ sample.

Fig. 7 shows the capacity change with increasing charge/discharge cycle number for $\text{Na}_2\text{Ti}_{3-x}\text{V}_x\text{O}_7$ up to 1000 cycles. Although the V substitution has a negative effect on the capacity of $\text{Na}_2\text{Ti}_3\text{O}_7$, this material has a very good capacity retention property since its capacity remains almost constant between 300 and 1000th cycles. Even with the addition of vanadium, the crystal structure of the materials is stable upon charging/discharging. We have used both the main

matrix and the nanorods to fabricate the electrodes. Fig. 7 shows that the pristine sample has 110 mA h g^{-1} and 42 mA h g^{-1} for the 1st and 1000th cycles, respectively.

3.3. Degradation mechanism

The crystal structure of the active materials plays a crucial role in the battery performance. Investigations of the structural deformation during charge/discharge are expected to reveal the structural factors behind the capacity fade. Insertion/removal of the Na ions from the active materials causes changes in the crystal structure. Upon multiple repetitions of this process, these structural modifications become irreversible and detrimental for the battery life.



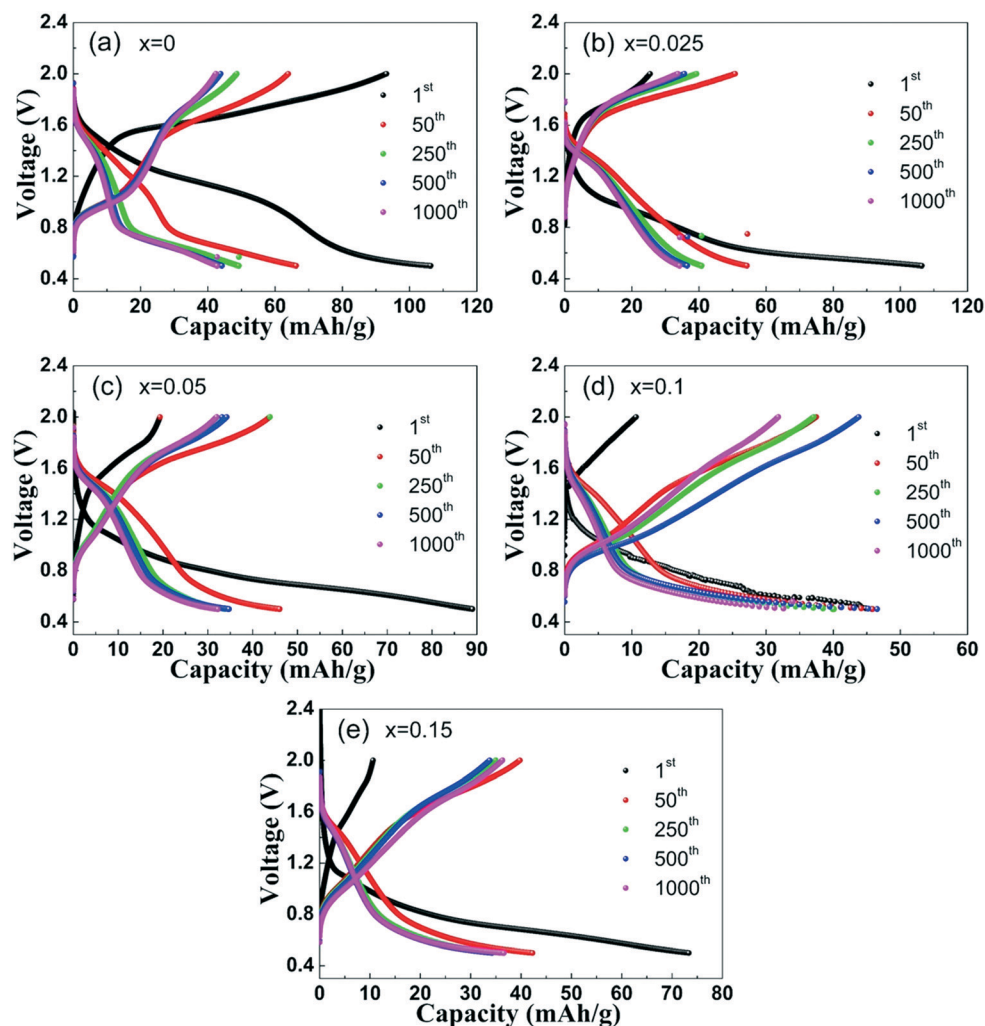


Fig. 6 Capacity–voltage graphs of nominal $\text{Na}_2\text{Ti}_{3-x}\text{V}_x\text{O}_7$ compositions ($x = 0, 0.025, 0.05, 0.1$ and 0.15).

The *ex situ* XRD data of the electrode materials after 1000 cycles as presented in Fig. 8 reveal impurity phases such as TiO , TiO_2 and Ti_7O_{13} .

We also performed *ex situ* XAS measurements after the 1st, 25th, 50th, 100th and 500th cycles for the $x = 0.10$ sample to

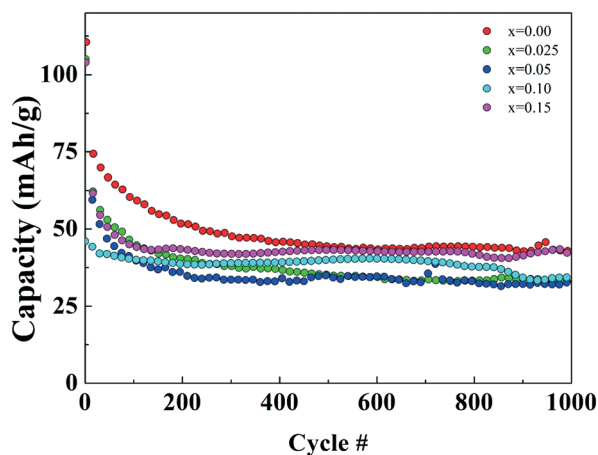


Fig. 7 Capacity change with cycle number of nominal $\text{Na}_2\text{Ti}_{3-x}\text{V}_x\text{O}_7$ compositions ($x = 0, 0.025, 0.05, 0.1$ and 0.15).

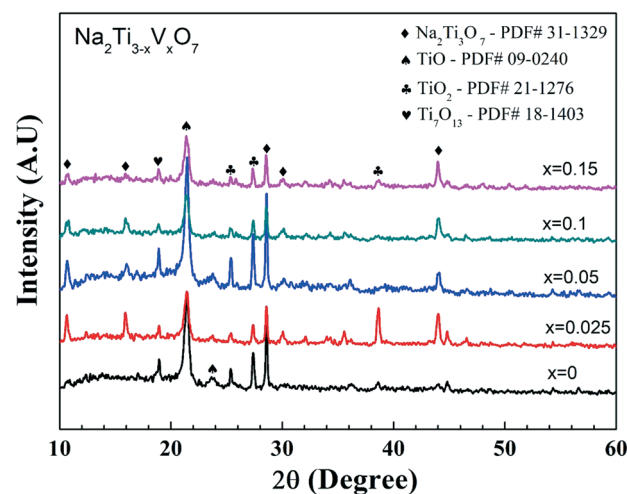


Fig. 8 *Ex situ* XRD data of nominal $\text{Na}_2\text{Ti}_{3-x}\text{V}_x\text{O}_7$ ($x = 0, 0.025, 0.05, 0.1$ and 0.15) compounds after 1000 cycles.



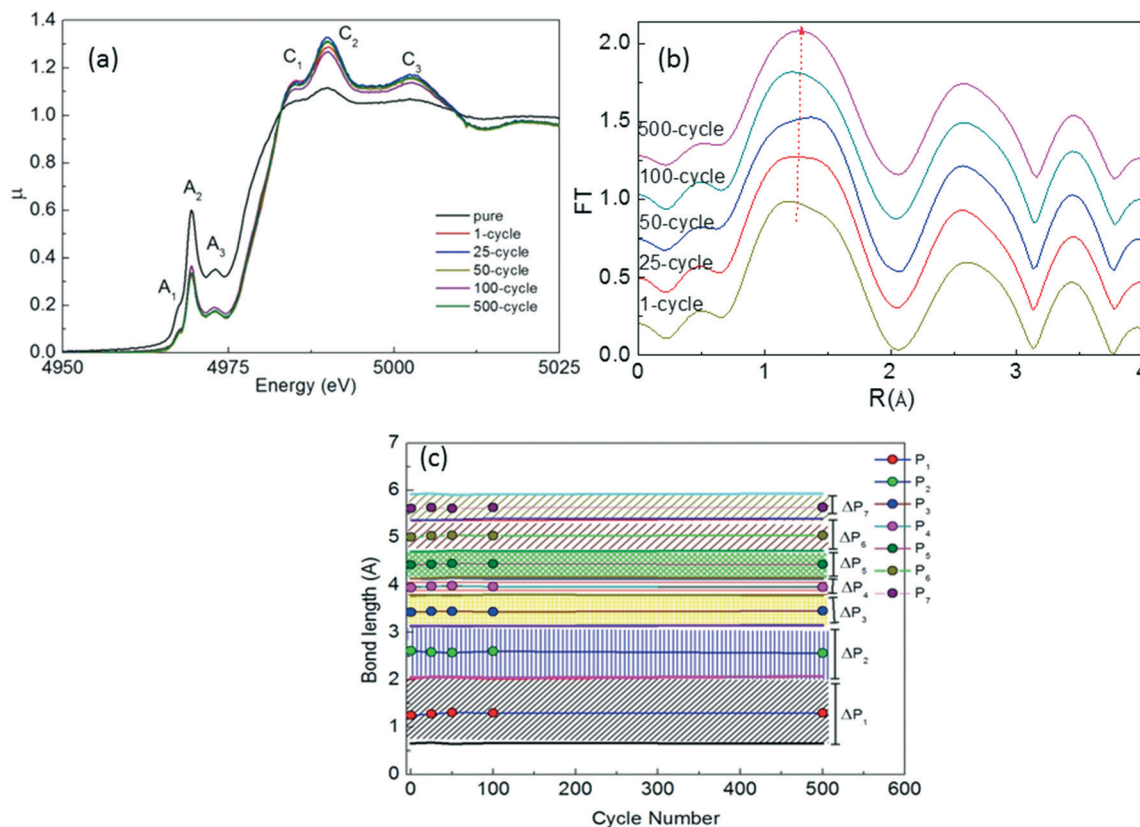


Fig. 9 (a) XAFS spectra, (b) FT graphs and (c) peak positions and ΔP values (in FT graphs) of $x = 0.10$ $\text{Na}_2\text{Ti}_3\text{O}_7$ after 500 cycles.

determine the major structural changes upon repeated cycling as seen in Fig. 9. We have observed 6 different peaks in the XAFS data as observed in uncycled samples (Fig. 5(a)). C_1 , C_2 and C_3 peaks have relatively higher intensity than those of the uncycled samples and the cycling process changes the spectrum slightly. The change in the intensity of the C-signed peaks in the XAFS data is related to formation of TiO_2 , TiO and Ti_7O_{13} phases since the environment of Ti ions change with the

formation of these phases. In addition, the FT data show a similar behavior with the uncycled sample. It is clear that the main phase remains to be present upon cycling and the bond lengths of impurity phases as shown in the XRD graph (Fig. 8) should be the same length in the existing peaks of the main phase as seen in Fig. 9(b) and (c).

TEM was used to look at the nature of structural changes that occur during cycling. In Fig. 10 we show the TEM images of a nanorod of the $x = 0.10$ sample 'before' and 'after' 1000 cycles. The 'before' sample has a clean overall appearance (top left), and the high resolution image (top right) has a uniform crystalline appearance up to the surface. The 'after' sample (bottom left) shows variations in intensity across its width and there is an extra material attached to the surfaces. The high resolution image (bottom right) shows loss of crystallinity. The interplanar spacing measured in the 'before' material was 0.82 nm, the same within error as reported in Fig. 3. In the 'after' material, the spacing lies in the range of 0.68 to 0.70 nm. This clearly shows the structural deformation upon repeated cycling.

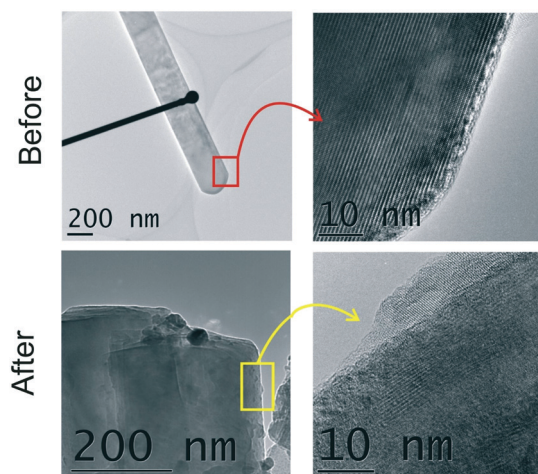


Fig. 10 TEM images of a nanorod of the $x = 0.10$ sample before cycling and after 1000 cycles.

Conclusions

In this work we report the solid state synthesis of $\text{Na}_2\text{Ti}_3\text{O}_7$ nanorods *via* a defect assisted route upon V addition. Among the nominal $\text{Na}_2\text{Ti}_{3-x}\text{V}_x\text{O}_7$ compositions where $x = 0.0, 0.025, 0.05, 0.1$ and 0.15 , we observed that the pristine sample ($x =$



0.0) has the bulk form while addition of even a small amount of V in the nominal composition causes formation of nanorods. Our TEM-EDS analysis shows that the nanorods do not contain any vanadium. We attribute the growth of the nanorods to a defect assisted growth mechanism which confirms our claim regarding the catalytic role of vanadium in the nanorod growth. We have also tested battery performances of our samples. The $x = 0.10$ sample shows the best capacity retention among all the samples, therefore we have examined the capacity fade mechanism of this sample *via ex situ* XRD, XAS and TEM studies. We found that repeated cycling causes formation of various titanium oxide phases and significant morphological deformations.

Conflicts of interest

There are no conflicts to declare.

Acknowledgements

This project was supported by the Inonu University Research Council with contract number of BAP-2015/85. Dr. S. Demirel was supported by the TUBITAK 2214-A International scholarship program. Synchrotron and TEM studies were performed through funding from the EU-H2020 research and the innovation program under grant agreement No. 654360 having benefitted from the access provided by DESY in Germany and by Lund University in Sweden within the framework of the NFFA-Europe Transnational Access Activity.

References

- V. L. Chevrier and G. Ceder, *J. Electrochem. Soc.*, 2011, **158**, A1011.
- Y. Liu, Z. Sun, K. Tan, K. D. Di, J. Sun, L. Liang, L. Hou and C. Yuan, *J. Mater. Chem. A*, 2019, **7**, 4353–4382.
- C. Yang, Y. Liu, X. Sun, Y. Zhang, L. Hou, Q. Zhang and C. Yuan, *Electrochim. Acta*, 2018, **271**, 165–172.
- P. Senguttuvan, G. Rousse, V. Seznec, J.-M. Tarascon and M. R. Palacin, *Chem. Mater.*, 2011, **23**, 4109–4111.
- J. Ni, S. Fu, C. Wu, Y. Zhao, J. Maier, Y. Yu and L. Li, *Adv. Energy Mater.*, 2016, **6**, 1502568.
- Z. Zhang, J. B. M. Goodall, S. Brown, L. Karlsson, R. J. H. Clark, J. L. Hutchison, I. U. Rehman and J. A. Darr, *Dalton Trans.*, 2010, **39**, 711–714.
- Y. V. Kolen'ko, K. A. Kovnir, A. I. Gavrilo, A. V. Garshev, J. Frantti, O. I. Lebedev, B. R. Churagulov, G. Van Tendeloo and M. Yoshimura, *J. Phys. Chem. B*, 2006, **110**, 4030–4038.
- W. Zou, J. Li, Q. Deng, J. Xue, X. Dai, A. Zhou and J. Li, *Solid State Ionics*, 2014, **262**, 192–196.
- H. Pan, X. Lu, X. Yu, Y.-S. Hu, H. Li, X.-Q. Yang and L. Chen, *Adv. Energy Mater.*, 2013, **3**, 1186–1194.
- M. Xie, K. Wang, R. Chen, L. Li and F. Wu, *Chem. Res. Chin. Univ.*, 2015, **31**, 443–446.
- C. Ding, T. Nohira and R. Hagiwara, *J. Power Sources*, 2017, **354**, 10–15.
- C. Jiang, E. Hosono and H. Zhou, *Nano Today*, 2006, **1**, 28–33.
- Y. Sun, N. Liu and Y. Cui, *Nat. Energy*, 2016, **1**, 16071.
- P. Poizot, S. Laruelle, S. Grugeon, L. Dupont and J. M. Tarascon, *Nature*, 2000, **407**, 496–499.
- C.-K. Ho, C.-Y. V. Li and K.-Y. Chan, *Ind. Eng. Chem. Res.*, 2016, **55**, 10065–10072.
- B. H. Toby and R. B. Von Dreele, *IUCr, J. Appl. Crystallogr.*, 2013, **46**, 544–549.
- Y. Wang, H. Li, P. He, E. Hosono and H. Zhou, *Nanoscale*, 2010, **2**, 1294.
- T. Kawamura, M. Makidera, S. Okada, K. Koga, N. Miura and J. Yamaki, *J. Power Sources*, 2005, **146**, 27–32.
- M. Xu, Y. Niu, C. Chen, J. Song, S. Bao and C. M. Li, *RSC Adv.*, 2014, **4**, 38140–38143.
- P. Slamet, W. B. Widayatno, A. Subhan and B. Prihandoko, *IOP Conf. Ser.: Mater. Sci. Eng.*, 2018, **432**, 012058.
- A. Rudola, K. Saravanan, C. W. Mason and P. Balaya, *J. Mater. Chem. A*, 2013, **1**, 2653.
- A. L. Sauvet, S. Baliteau, C. Lopez and P. Fabry, *J. Solid State Chem.*, 2004, **177**, 4508–4515.
- Crystal Growth - From Fundamentals to Technology*, ed. G. Müller, J. J. Metois and P. Rudolph, Elsevier, 2004.
- H. Yung-Jung and S.-Y. Lu, *J. Phys. Chem. B*, 2005, **106**, 4398–4403.
- H. K. Yu and J.-L. Lee, *Sci. Rep.*, 2015, **4**, 6589.
- V. Palomares, M. Casas-Cabanas, E. Castillo-Martínez, M. H. Han and T. Rojo, *Energy Environ. Sci.*, 2013, **6**, 2312.
- Y. S. Park, S.-H. Lee, J.-E. Oh, C.-M. Park and T.-W. Kang, *J. Cryst. Growth*, 2005, **282**, 313–319.
- S. Demirel, E. Oz, E. Altin, S. Altin, A. Bayri, P. Kaya, S. Turan and S. Avci, *Mater. Charact.*, 2015, **105**, 104–112.
- A. Niltharach, S. Kityakam, A. Worayingyong, J. Thienprasert, W. Klysubun, P. Songsiriththigul and S. Limpijumngong, *Phys. B*, 2012, **407**, 2915–2918.
- F. Farges, G. E. Brown and J. J. Rehr, *Phys. Rev. B: Condens. Matter Mater. Phys.*, 1997, **56**, 1809–1819.
- C. Hennig, G. Reck, T. Reich, A. Roßberg, W. Kraus and J. Sieler, *Z. Kristallogr.*, 2003, **218**, 37–45.
- P. Li, W. Wang, S. Gong, F. Lv, H. Huang, M. Luo, Y. Yang, C. Yang, J. Zhou, C. Qian, B. Wang, Q. Wang and S. Guo, *ACS Appl. Mater. Interfaces*, 2018, **10**, 37974–37980.

